The Journal of Experimental Biology 208, 1079-1094
Published by The Company of Biologists 2005
doi:10.1242/jeb.01471

The aerodynamics of *Manduca sexta*: digital particle image velocimetry analysis of the leading-edge vortex

Richard J. Bomphrey[1,*], Nicholas J. Lawson[2], Nicholas J. Harding[1], Graham K. Taylor[1] and Adrian L. R. Thomas[1]

[1]*Department of Zoology, University of Oxford, South Parks Road, Oxford, OX1 3PS, UK* and [2]*College of Aeronautics, Cranfield University, Cranfield, MK43 0AL, UK*

*Author for correspondence (e-mail: Richard.Bomphrey@zoology.oxford.ac.uk)

Accepted 21 December 2004

Summary

Here we present the first digital particle image velocimetry (DPIV) analysis of the flow field around the wings of an insect (the tobacco hawkmoth *Manduca sexta*, tethered to a 6-component force–moment balance in a wind tunnel). A leading-edge vortex (LEV) is present above the wings towards the end of the downstroke, as the net upward force peaks. Our DPIV analyses and smoke visualisations match the results of previous flow visualisation experiments at midwing, and we extend the experiments to provide the first analysis of the flow field above the thorax. Detailed DPIV measurements show that towards the end of the downstroke, the LEV structure is consistent with that recently reported in free-flying butterflies and dragonflies: the LEV is continuous across the thorax and runs along each wing to the wingtip, where it inflects to form the wingtip trailing vortices. The LEV core is 2–3 mm in diameter (approximately 10% of local wing chord) both at the midwing position and over the centreline at 1.2 m s^{-1} and at 3.5 m s^{-1} flight speeds. At 1.2 m s^{-1} the measured LEV circulation is 0.012±0.001 m^2 s^{-1} (mean ± S.D.) at the centreline and 0.011±0.001 m^2 s^{-1} halfway along the wing. At 3.5 m s^{-1} LEV circulation is 0.011±0.001 m^2 s^{-1} at the centreline and 0.020±0.004 m^2 s^{-1} at midwing. The DPIV measurements suggest that if there is any spanwise flow in the LEV towards the end of the downstroke its velocity is less than 1 m s^{-1}. Estimates of force production show that the LEV contributes significantly to supporting body weight during bouts of flight at both speeds (more than 10% of body weight at 1.2 m s^{-1} and 35–65% of body weight at 3.5 m s^{-1}).

Key words: flow visualisation, leading-edge vortex, *Manduca sexta*, hawkmoth, DPIV, particle image velocimetry, PIV, unsteady aerodynamics, flapping flight, micro air vehicle.

Introduction

A quantitative description of the flow field around insect wings is fundamental to understanding the aerodynamics of insect flight. The high performance of flying insects implies aerodynamic forces larger than could be accounted for by conventional attached-flow aerodynamics (Sane and Dickinson, 2002; Weis-Fogh, 1973; Zbikowski, 2002). Recent experiments with tethered hawkmoths and large-scale mechanical flapping models have successfully replicated at least some of the force-generating abilities of free-flying insects (Birch and Dickinson, 2001; Dickinson et al., 1999; Ellington et al., 1996; Maxworthy, 1981; Van den Berg and Ellington, 1997a). In both hawkmoths and mechanical models, a leading-edge vortex (LEV) formed above the wing during the downstroke has been implicated in most, if not all, of the necessary lift enhancement over conventional steady state mechanisms. Here, we provide the first detailed quantitative measurements of the flow velocities and vorticity in the LEV of a real insect, and use this to assess quantitatively the consequences of the LEV for lift production.

A vortex held above a wing has long been known to be capable of enhancing lift (Gad-el-Hak and Ho, 1985; Gursul et al., 1994; Huang and Chow, 1982; Mourtos and Brooks, 1996; Riddle et al., 1999; Rossow, 1978, 1992, 1994; Saffman and Sheffield, 1977). A transient LEV can be formed over an aerofoil by sudden changes in flow velocity or pitch (Délery, 2001). Aerodynamic experiments in unsteady flows have shown that the vortex can provide a transient increase in the lift coefficient by as much as an order of magnitude above the steady state value for a given aerofoil (Délery, 2001; Gad-el-Hak and Ho, 1985; Gursul et al., 1994; Mourtos and Brooks, 1996). Studies with mechanical models (Birch and Dickinson, 2001; Dickinson et al., 1999; Van den Berg and Ellington, 1997a) suggest that LEVs can be quite stable over model insect wings, and may produce a twofold increase in lift, but there has been considerable debate over the exact structure of the

LEV and how LEV stability is maintained for the duration of the downstroke.

Structure of the LEV

Three distinct categories of insect LEV structure have been described on the basis of studies with real insects and mechanical flapping models. These three categories of LEV are summarised in Fig. 1. This paper aims to test which of these flow-fields actually applies in *Manduca*. The differences between these flow-fields are non-trivial. The three categories of LEV have qualitatively different flow topologies, corresponding to qualitatively different local solutions to the Navier–Stokes equations (Thomas et al., 2004). Moreover, because the topology of the vortex differs qualitatively between the three categories of LEV structure, the overall size of the vortex and its contribution to the total lift generated by the animal can only be calculated correctly if the correct topology is used. It is therefore essential that we distinguish between these different topological models of the flow-field if we are to generate predictive, analytical models of LEV insect flight aerodynamics

Structure and stability of the LEV: Class I

The LEV was first implicated in insect high lift mechanisms by Maxworthy on the basis of experiments with flapping mechanical models (Maxworthy, 1979). Maxworthy's description of the structure of the LEV is complex (Fig. 1A). Because the left and right wings of Maxworthy's flapper did not form a continuous lifting surface, trailing vortices were formed at the wing roots as well as at the wing tips. This is arguably somewhat unnatural, but might correspond to the situation in insects such as craneflies (Diptera: Tipulidae) with highly petiolated wings. With this class of vortex structure, a LEV is formed on both wings, and is continuous with the trailing vortices at the wing root and wing tip. Its flows are strongly three-dimensional with an axial flow along the core from root to tip along much of the wing. At the wingtip this axial flow trails off into the wingtip trailing vortices, which form part of a closed vortex loop connecting the two wingtips. A second trailing vortex connects the two wing-roots, thereby completing the vortex loop, which is highly deformed relative to the classical elliptical form assumed in most vortex models of animal flight. This connection between contralateral wing root vortices was clearly visualised in Maxworthy's model experiments. Joining the wingtip and wing root vortices to complete the vortex loop is a necessary feature of the type of flow topology that Maxworthy describes (unless, of course, the wings act completely independently, each forming a discrete vortex loop) and follows from Kelvin's fundamental laws of vortices, which require that all vortices either form continuous loops, or end at a surface. In this paper, Maxworthy's description of vortex structure will be referred to as a Class I LEV (Fig. 1A).

Maxworthy showed that the LEV was responsible for a substantial enhancement of lift – in fact, for the majority of the lift. Using a quasi-steady approximation he estimated that in the presence of the LEV a lift coefficient of 6.8 could be sustained, providing more than twice the lift required to support the weight of the Chalcid wasp *Encarsia formosa* he was modelling. The stability of the Maxworthy LEV depends crucially on the axial flow along the vortex core because this flow transports vorticity away from the leading edge along the wing and out into the wingtip vortices (axial flow is marked by orange arrows in Fig. 1). He suggested that if this axial flow were absent, the LEV would grow rapidly and be shed into the wake, as happens in the 2D situation where the wake forms a reverse Kármán vortex street (Maxworthy, 1979, 1981).

Structure and stability of the LEV: Class II

The second description of a LEV (and the first visualisation of a LEV generated by a real insect) was by Luttges' group, in a series of studies with tethered dragonflies (Reavis and Luttges, 1988; Somps and Luttges, 1985) and tethered hawkmoths (Luttges, 1989). Luttges' group were also able to reproduce the features of the flow field they observed using mechanical flappers (Kliss et al., 1989; Reavis and Luttges, 1988; Somps and Luttges, 1985). The presence of a LEV was clearly revealed in smoke visualisations (summarised in Luttges, 1989) of both hawkmoths and dragonflies. The structure differed from Maxworthy's results (Maxworthy, 1979) in two ways. Firstly, there was no root vortex, because the visualisations showed that the LEV was continuous across the thorax (Luttges, 1989). Secondly, in contrast to Maxworthy (1979), Luttges' simultaneous flow visualisations from top and side views with both dragonflies and hawkmoths show little evidence of spanwise flows at any stage in the wingbeat. Luttges argued that the absence of spanwise flow was a genuine, and general, feature of the flows his insects generated, stating that '*the flow structure of the vortices is largely two-dimensional while in the presence of the wing (or wings) that produce them*' (p. 454, Luttges, 1989). Specific detail of the flow topology around the wings and over the thorax was not drawn explicitly by Luttges, but the description appears to be topologically similar to that described more recently by Srygley and Thomas (2002) for free-flying butterflies, in that the LEV is continuous across the thorax.

Srygley and Thomas (2002) visualised the flow around the butterfly *Vanessa atalanta*, and went on to define the topology in the descriptive framework provided by critical point theory (Lighthill, 1963; Perry and Chong, 2000). In the case of *Vanessa*, the LEV flow topology appears to have a free-slip critical point (a 3D focus) over the centreline (and therefore no surface-bound foci on the wings). A topology consistent with both Luttges' results for hawkmoths (Luttges, 1989) and Srygley and Thomas' results for *Vanessa* (Srygley and Thomas, 2002) is shown in Fig. 1B and will be known as a Class II LEV in this paper.

The flow field differs from Maxworthy's in two ways. Firstly, although the LEV above the thorax in Luttges' and in Srygley and Thomas's work (Fig. 1B) looks superficially similar to the wing root vortices in Maxworthy's LEV (Fig. 1A), the flow topology differs qualitatively in this region.

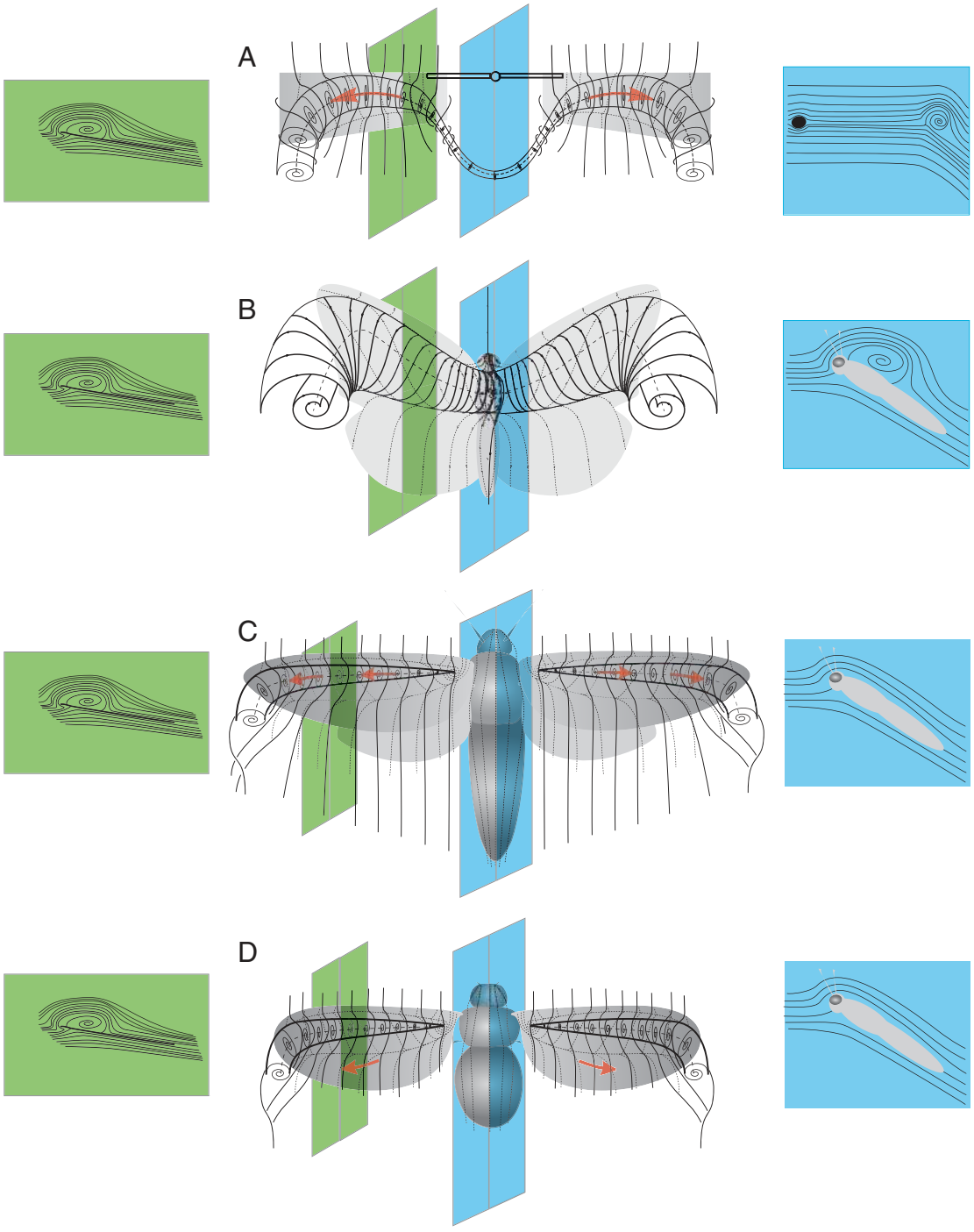

Fig. 1. The three classes of leading-edge vortex (LEV) that have been described to date. (A) Class I: the Maxworthy (1979) description from his model experiments based on the 'fling' of the chalcid wasp *Encarsia formosa.* The LEV inflects into tip and root vortices on each wing. The tip vortices connect to form a vortex ring behind the model, and the root vortices also connect so that the wake consists of one continuous vortex loop of complex shape. (B) Class II: the structure described by Luttges (1989) with a single LEV extending across the thorax of a hawkmoth and inflecting to form both tip vortices. This structure implies a free-slip critical point (a 3D focus) over the centreline of the thorax, as described by Srygley and Thomas (2002) for butterflies *Vanessa atalanta*. The topology is similar to that in A except that the root vortex is replaced by a continuous LEV over the thorax and there is no significant spanwise flow. (C) Class III: the structure described by Ellington and colleagues (Ellington et al., 1996; Van den Berg and Ellington, 1997a) where the LEV on *Manduca* is similar to that found on a delta wing. In this model there must be a surface-bound focus at the base of each wing and attached flow over the thorax. (D) Also Class III: the flow, topologically similar to C, scaled for *Drosophila* by Birch and Dickinson (2001). The flows in C and D differ qualitatively from A and B in the absence of the linkage between the LEVs *via* either wing root vortices or a continuation of the LEV across the centreline. Spanwise (axial) flow, if present, is marked by orange arrows in each case. Vertical planes show the simplified flow topology at the centreline and midwing positions.

Whereas Luttges' and Srygley and Thomas' vortex is bound to a surface, Maxworthy's root vortex is not. This prevents this portion of the vortex from generating any useful lift, and renders it unstable because of its tendency to convect freely with the flow. Secondly, Maxworthy suggested that spanwise flow was essential to transport vorticity out of the LEV and into the wake so that the LEV does not grow too large to remain on the wing during the downstroke. In contrast Srygley and Thomas (2002) and Taylor et al. (2003) have suggested that the wingbeat kinematics are tuned to operate at an appropriate Strouhal number *St*, such that the LEV grows throughout the downstroke, but not so much as to be shed before stroke reversal (where *St* is defined as wingbeat frequency multiplied by the wingtip excursion divided by the freestream velocity). In other words, whereas axial flow is necessary for a LEV to persist indefinitely (as on a delta wing aircraft, or non-reciprocating wing on a whirling arm; Usherwood and Ellington, 2002), axial flow is unnecessary if the wingbeat period is shorter than the timescale on which the vortex would naturally become unstable. This effect has been demonstrated in many experiments and theoretical investigations with flapping, pitching and plunging wings (Jones and Platzer, 1996; Lewin and Haj-Hariri, 2003; Taylor et al., 2003; Triantafyllou et al., 1993, 1991; Tuncer and Platzer, 1996; Wang, 2000).

Structure and stability of the LEV: Class III

The third description of a LEV came from detailed analyses by Ellington's group. In contrast to Luttges and colleagues, they emphasized the 3D nature of the LEV (Ellington et al., 1996; Van den Berg and Ellington, 1997a,b; Willmott et al., 1997). In tethered hawkmoths Willmott et al. (1997) and Ellington et al. (1996) used smoke visualisations to show that a small LEV was present on the downstroke at flight speeds from 0.4 m s^{-1} to 5.7 m s^{-1}, at positions from 0.25 *R* (1/4 wing length, *R*) outboards, and the LEV was larger at higher speeds. Detailed analysis of the flow visualisation images at 1.8 m s^{-1} showed that the LEV was absent at 0.25 *R*, visible at 0.5 *R* (midwing), and larger at 0.75 *R*. The LEV broke away from the surface close to 0.75 *R* and rolled up with the wingtip vortices (see fig. 5 and accompanying text in Willmott et al., 1997). No analysis of the flow over the centreline was published, but the authors suggest that the absence of evidence of a LEV at 0.25 *R* implies that the LEV grows along the wing in a conical structure [Luttges' results (Luttges, 1989) showing a LEV over the thorax were dismissed as unnatural on the basis that he reported the observation of high lateral forces during some sequences when the moth was struggling to escape the tether]. The flow topology described by Ellington's group (Ellington et al., 1996; Van den Berg and Ellington, 1997a) is represented in Fig. 1C and will be known as a Class III LEV in this paper.

Ellington and colleagues describe the Class III LEV as '*a conical spiral, enlarging as it is swept along the wing by an axial (spanwise) flow*', stating that: '*The conical, spiral vortex of the flapper is, in fact, remarkably similar in form to that over delta wings*' (Ellington et al., 1996). The vortices over a delta wing originate from a focus attached to the wing base (apex), and the expectation in such a situation is therefore that no vortical structure will be present between the wing bases. Willmott et al. (1997) were unable to visualise smoke streams within the LEV itself using tethered moths, and relied instead on results from a large-scale mechanical flapper for further detail (Van den Berg and Ellington, 1997a,b). Results with the flapper showed that the LEV diameter was just under 2 cm at 0.25 *R*, 3.5 cm at 0.5 *R* LEV, and 4 cm at 0.63 *R* (Van den Berg and Ellington, 1997b). This means that at midwing, the LEV core diameter is approximately 30% of the wing chord.

The stability of the flow field around the hawkmoth flapper is apparently analogous to that of the LEVs over delta wings, with vortex growth limited by the removal of vorticity through a spanwise axial flow along the vortex cores (Ellington et al., 1996; Van den Berg and Ellington, 1997a). Ellington et al. (1996) and Van den Berg and Ellington (1997) attempted to quantify the properties of the LEV on their flapper. Spanwise flow, circulation and vortex diameter were all estimated from video smoke visualisation, from which it was concluded that the LEV could produce up to 2/3 of the total lift required for flight (Van den Berg and Ellington, 1997). However, given the problems of interpreting flow visualisations (Hama, 1962), direct measurement of velocity would provide a more accurate way of determining the circulation of the LEV.

Studies by Dickinson and colleagues (Birch and Dickinson, 2001; Dickinson et al., 1999) of scaled model wings at Reynolds numbers appropriate for *Drosophila* revealed a spiral LEV of similar structure to that found on Ellington et al.'s flapper (Fig. 1D). The results suggested, however, that spanwise flow was unnecessary in stabilising the LEV, as chordwise fences placed on the leading edge of the wing to prevent this flow reduced the size of the LEV, but did not render it unstable. Thus, while there inevitably must be some element of spanwise flow in any conical LEV with an attached focus near the wing root, there is still uncertainty over the need for a spanwise component to maintain vortex stability. Whether or not spanwise flow is a significant feature of the flow-field, the results of the Ellington and Dickinson groups alike are consistent with the interpretation given above, that a LEV can be made to persist over the wing for the duration of the downstroke, provided that the kinematics are configured to an appropriate Strouhal number.

Comparison with previous work: Manduca *smoke flow visualisations*

In order to directly compare our results with previously published studies of *Manduca* (Willmott et al., 1997), we first captured images of smoke trails as they arrived at the midwing position of a tethered moth. We used the smoke-wire technique, which is similar to the smoke-rake technique of Willmott et al. (1997), but provides higher spatial resolution. A crimped Nichrome wire placed at the upstream end of the windtunnel's working section was coated with Johnson's Baby Oil. Mild Ohmic heating caused the oil to burn off at the

narrower crimped sections of the wire and be transported with the flow along the windtunnel toward the subject in a vertical plane of closely spaced, discrete smoke trails emanating horizontally from the wire.

Our smoke visualisations confirm the results of Willmott et al. (1997), with a leading edge vortex over the wings at the midwing position on the downstroke. The smoke rolls up into the leading-edge vortex as the vortex grows through the downstroke and subsequently sheds into the wake (Fig. 2). Our smoke visualisations show a flow pattern that matches the leading edge vortex Willmott et al. (1997) describe in structure, position and size relative to the wing. Following examination of the midwing flow, we were able to capture images of the flow over the centreline of the moth (sagittal plane of symmetry; Fig. 3). The flow remains attached for most of the downstroke, as was the case for the closest inboard position visualised in Willmott et al. (1/4 wing length). However, as the wings approach stroke reversal (Fig. 3B,C) the flow detaches forming a separated flow region above the centreline. Wilmott et al. (1997) were careful not to specify the nature of the flow over the centreline, because they had not been able to visualise the flow in that region, but the delta wing analogy they made (see above) implies that the flow should be attached between the wing bases. Separation over the centreline suggests a fundamentally different flow topology for *Manduca*. To corroborate the conclusions from the smoke wire flow visualisation, and to quantify the flows therein, we use DPIV to explore the velocity field around the wings and over the centreline of *Manduca*.

DPIV: objectives

In what follows, 2D digital particle image velocimetry (DPIV) is used to measure and analyse the flow field around the wings of tethered hawkmoths. DPIV can record planar instantaneous high-resolution vector maps of flow velocity and vorticity. Instantaneous planar streamlines can also be estimated from the data thus providing an objective picture of selected planes in the flow field. Hence 2D DPIV can be used to directly measure the strength and size of the in-plane LEV structures discussed previously. 2D DPIV cannot be used directly to measure the strength of spanwise flow, which occurs out of plane. Nevertheless, what distinguishes between the three classes of LEV proposed above is not so much the presence or absence of spanwise flow, but the exact topology of the flow in terms of its critical points (Srygley and Thomas, 2002; Thomas et al., 2004). 2D DPIV can be used to infer the number, location and kind of these critical points, and is used to this end below.

The major distinguishing feature for all three classes of LEV is the flow topology at the insect centreline. If a Class I LEV is present, there will be a wing-root vortex (not bound to any surface) at the centreline, and the corresponding 2D DPIV velocity vector map will show a vortex structure not bound to the surface. If a Class II LEV is present, the LEV will continue bound across the centreline and the corresponding 2D DPIV velocity vector map will show a vortex structure bound to the

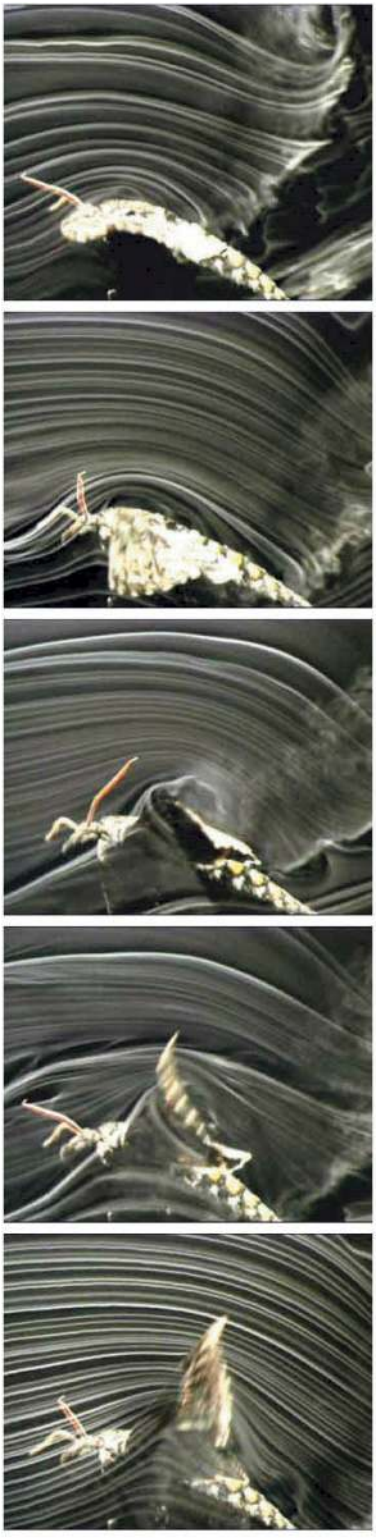

Fig. 2. Smoke wire flow visualisations of tethered *Manduca sexta*. The plane of the undisturbed smoke streams is coincident with the midwing position. The flow pattern is essentially indistinguishable from the results presented previously (Willmott et al., 1997; Ellington et al., 1996). There is a stagnation point on the underside of the wing, flow separates at the leading edge and reattaches towards the trailing edge, with an LEV in the separated flow region above the top surface of the wing.

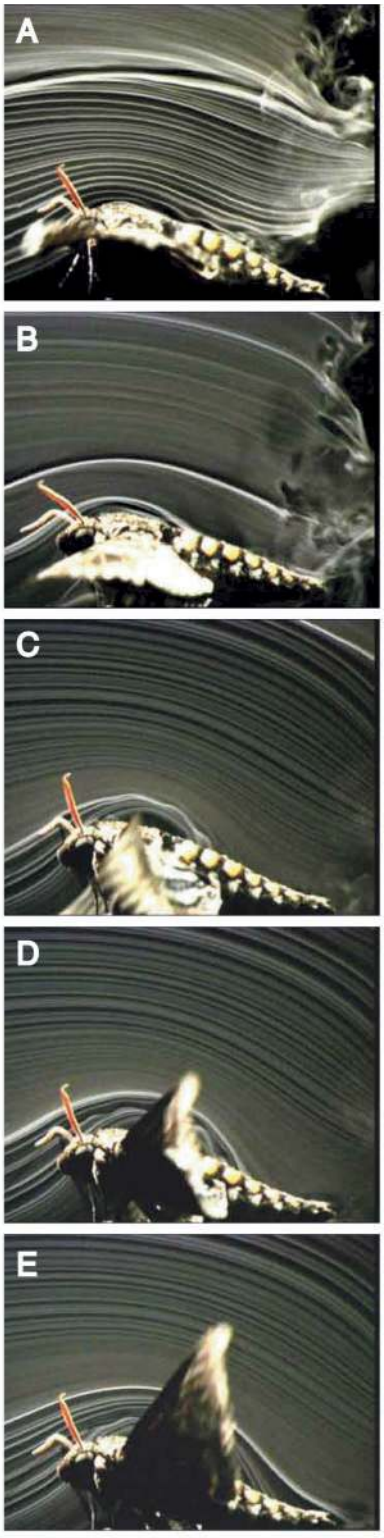

Fig. 3. Smoke wire visualisation of tethered *Manduca sexta* with the plane of the undisturbed smokestreams coincident with the thorax, close to the centreline. Flow is attached for the majority of the downstroke but separates at the end of the downstroke (images C–E); the separation has the same size and form as that containing an LEV in Fig. 2, and in previously published flow visualisations of outboard positions along the wing (Willmott et al., 1997; Ellington et al., 1996). The centreline position has not previously been analysed by flow visualisation.

surface. Finally if a Class III LEV is present, the LEV will have no influence at the centreline, so no centreline vortex would be expected to be visualised in the corresponding 2D DPIV velocity vector map. If planar 3D DPIV data were recorded using stereoscopic DPIV (Prasad, 2000), then the different Class III LEV structures could be further be distinguished, as described by Dickinson's and Ellington's groups, by analysing the strength of spanwise flow midwing. Unfortunately, this type of DPIV system was unavailable for this study. The 2D planar measurements nevertheless allow us to distinguish between the three classes of LEV.

Materials and methods

Tobacco hawkmoths *Manduca sexta* L. were obtained from a captive bred population, selected for physical characteristics indicative of health (good wing condition, strong free-flight ability, etc.). Data presented here were collected over six consecutive bouts of flight from a single individual weighing 1.52 g, with a wing length of 52 mm and a thorax width of 8 mm. Tethered flight was examined at two speeds, and sampled across wingbeats by random interaction between camera frequency and wingbeat frequency. For direct comparison with previous work the body angle was set at 28° matching the value used by Willmott et al. (1997). Body angle was measured from a tangential line across the thorax at the base of wings using NIH image 1.61/ppc.

DPIV measurements were performed in a low-speed, low-turbulence wind tunnel (1.0 m×0.5 m×0.5 m working section) at 1.2 m s^{-1} and 3.5 m s^{-1}. The insect was tethered to a 6-component strain gauge force–moment balance (I-666; FFA Aeronautical Research Institute, Sweden; 10 kHz sampling rate) connected to a Macintosh computer (with MacLab hardware and Chart v.3.6/s) and synchronised with the DPIV system. The balance output was converted to force–moment units in Matlab, using a static calibration analysed as a General Linear Model (GLM), in which we retained significant terms up to third order in any one channel plus all significant second order interactions (P=0.05; G. K. Taylor and A. L. R. Thomas, manuscript in preparation). This conversion accounts for interactions between the orthogonal force–moment components resulting from non-orthogonalities intrinsic in the force balance architecture. The resonant frequency of the system is in excess of 550 Hz with the subject attached, and since this is well over an order of magnitude higher than the wingbeat frequency (~19 Hz), there should be no issues with the insect's wingbeat exciting resonance of the measuring system.

A JEM Hydrosonic 2000 seeder with 'long lasting' smoke fluid (Lancelyn Theatre Supplies, Oxford, UK) was used to produce seeding with a mean particle diameter of less than 10 μm. A New Wave Gemini Nd-YAG laser (New Wave Research Inc., Fremont, CA, USA) combined with plano-concave and plano-cylindrical lenses (focal lengths 50 mm and 75 mm, respectively) produced a 0.5 mm thick light sheet oriented vertically across the imaging area. The laser was

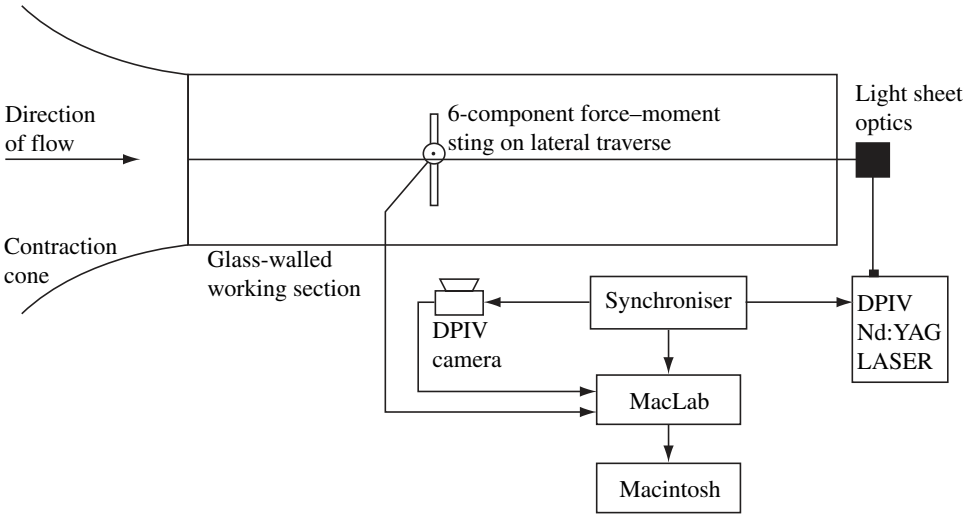

Fig. 4. Plan view schematic showing the windtunnel's working section and the positions of the camera and light sheet.

synchronised with a double frame digital camera (Kodak ES1.0 digital CCD, 1000^2 pixels) to record image pairs at up to 15 Hz (120 mJ per 5 ns pulse). To retain the particles within the light sheet, an optimised pulse separation interval of 120 µs at 3.5 m s^{-1} freestream velocity and 200 µs at 1.2 m s^{-1} was chosen. The light sheet was centred in the working section of the wind tunnel and a racked traverse moved the insect mount perpendicular to the light sheet to illuminate various stations across the wingspan (Fig. 4).

Dantec FlowManager software Dantec Dynamics, Skolvlunde, Denmark) was used to control the camera and laser for DPIV data acquisition. Images were processed using TSI UltraPIV Insight software incorporating the Hart Algorithm (Hart, 2000). A primary correlation window of 32×32 pixels was selected with a sub-correlation window of 16×16 pixels and a search radius of 8×8 pixels, and a bilinear peak search. This typically yielded 121×121 vectors per PIV image, corresponding to a spatial resolution of 0.75 mm×0.75 mm over a 92 mm×92 mm imaging area. Vector validation was performed in Insight (TSI Instruments, Bristol, UK), rejecting any vectors whose magnitude fell further than 3 standard deviations from the mean. Rejected vectors were replaced by vectors interpolated from the surrounding vectors in a 3×3 grid. Finally, the vectors were smoothed using the minimal smoothing allowed by the software (3×3 Gaussian smoothing, where adjacent vectors are weighted 40% relative to the target vector). Vector fields were displaced and vorticity values calculated using Tecplot v.8.0, where contour colours were added at a resolution consistent with the system's error (Lawson and Davidson, 2001). Streamlines were also added using Tecplot's Streamline Tool. In this case, as with the velocity vectors, the streamlines we present are confined to the 2D slice under interrogation. Streamline location and density were selected carefully by eye for maximum clarity of presentation.

For a 2D PIV system the velocity error originates from the recording and data processing stages. From error analysis outlined previously (Lawson and Davidson, 2001), it is estimated that the error in the PIV data is in the range 2.2–5.5% of full scale measurement, with the higher values occurring at the edge of the field of view due to perspective error (Reeves and Lawson, 2003). The colour bars have therefore been selected so that each step in colour represents 2–4% of the full scale measurement, which is approximately equal to the estimated error in the data, and greater than the error in the data in the region of interest in the flow field around the wings. Thus if a flow structure can be seen in colour shifts in the plots, it is most likely real. Raw data was analysed from original images that had zero or minimal glare. Solid bodies, such as the wings and thorax, can be a source of erroneous vectors and edge effects in the vector field. Original images of the moth were cut-and-pasted appropriately to mask the corresponding region of the vector plot. Edge effects may still be present outside of this region, but are sharply confined by the resolution of the system, because edge effects can only affect vectors calculated from a zone of interrogation overlapping an edge. Vectors within 0.75 mm of the wing or thorax should therefore be treated with caution, because their zone of interrogation will include an edge. Vectors within 1.5 mm of the wing or thorax could also be affected indirectly by edge effects because they are subject to 3×3 Gaussian smoothing with vectors affected directly by edge effects. All the flow features described in this paper are outside this small region of uncertainty.

For each flight session, 73 pairs of images were taken (limited by the computer's data storage capacity). At each windspeed, two flights were recorded with the light sheet in the sagittal plane of the animal, and two flights with the light sheet in a para-sagittal plane (midwing on the near wing).

Vortex identification

The identification of vortices has been the centre of much discussion, and there is considerable controversy in the aerodynamic literature over how to identify a vortex. One criterion is that streamlines spiral into a stable focus (Robinson, 1991); another is the presence of a vorticity

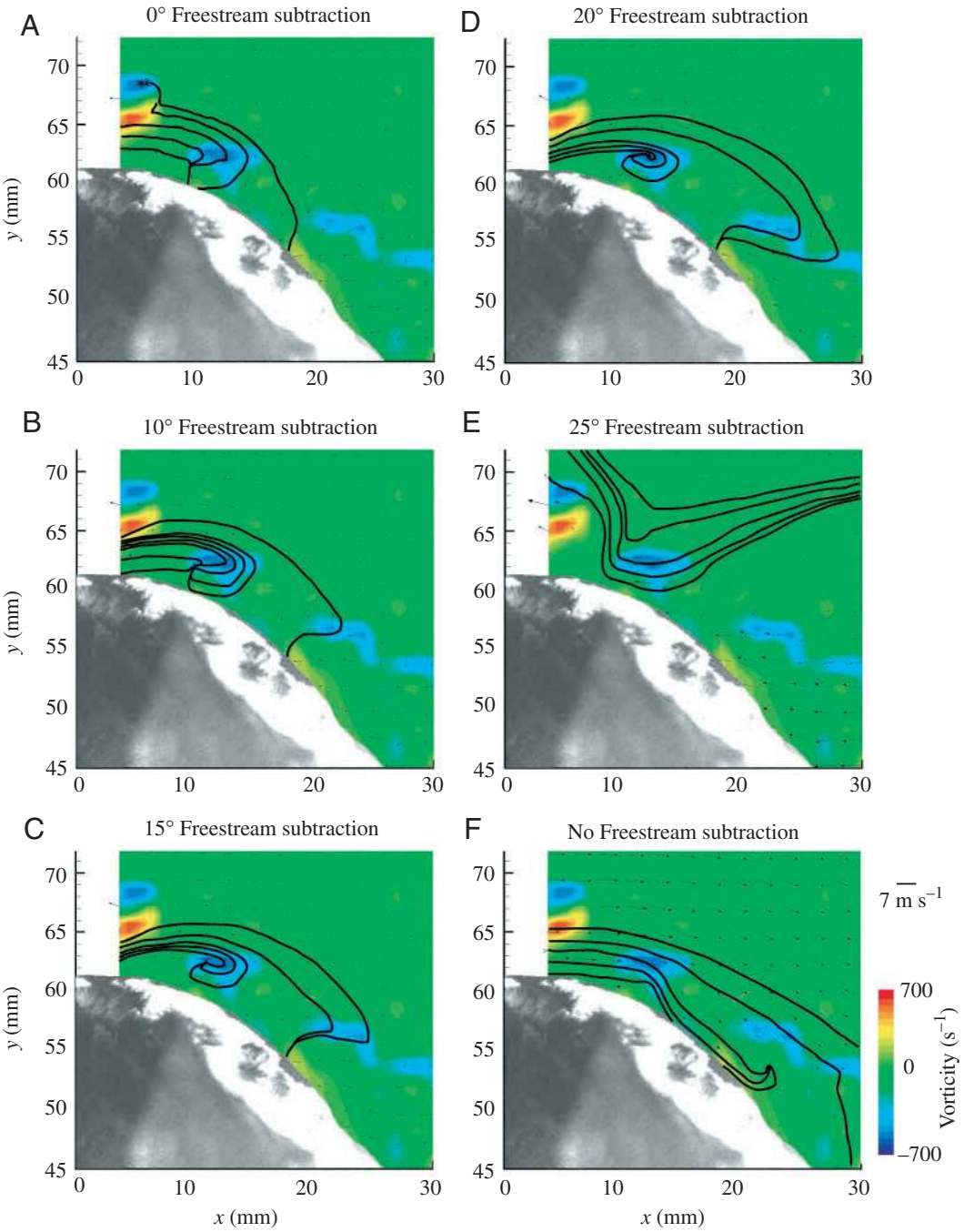

Fig. 5. The effect of vector subtraction on streamlines. No subtraction (F): this presents the measured data free from any manipulations, therefore the frame of reference is fixed with respect to the thorax and laboratory. Free stream subtraction 0° (A): here the velocity due to the windtunnel flow has been subtracted from the measured velocity vectors so that the frame of reference is fixed with respect to a distant particle in the flow, far enough away to be unaffected by the moth. These two cases represent the simplest manipulation of the data and transform the vector fields between two equally valid frames of reference – fixed with respect to the thorax of the moth, and fixed with respect to the distant fluid. However, it is not entirely clear that either of these two global frames of reference will be locally appropriate for resolving the LEV formed by a flapping wing. For flows that occur close to the surface of the animal, a locally valid frame of reference might be expected to take into account the local geometry of the body – so for, example, where the freestream is deflected as it flows around the body it would make sense, when looking for features in that flow, to subtract the freestream modified by its deflection around the body. Vorticity is unaffected by such frame of reference corrections, but now the frame of reference is a somewhat abstract concept – being fixed relative to distant fluid flowing with the freestream once it has been deflected by the body, but unaffected by the flow induced by the flapping wings. In the case shown here, a deflection of between 10° and 20° the frame of reference is adequate to see the streamlines converge to a focus coinciding with the peak in vorticity. The focus shifts from left to right during the iterations and then disappears altogether as it is transformed into a form only visible as a shear region.

maximum (Lugt, 1985a,b). Recommended practice is to use a combination of two or more criteria to reduce the likelihood of misidentification (Banks and Singer, 1995). Here we conclude that a vortex is present if the vector map yields streamlines that spiral into a focus, and the centre of that focus coincides with a vorticity maximum or minimum. The close match between the measured velocity and vorticity profiles and the theoretical predictions for a vortex provides confirmation that this procedure correctly identifies vortices.

Whenever a 2D slice is taken through a 3D flow field, it is imperative that the frame of reference is valid if a focus is to be visualised correctly. Here, we identify four valid frames of reference: two that are globally valid, and two that are only locally so. The first global frame of reference is provided by the raw vector data itself, and is fixed with respect to the camera. Vectors in this frame of reference result from the steady freestream velocity of the tunnel, the influence of the stationary moth's body, and the unsteady influence of the beating wings. A second global frame of reference may be generated by subtracting the freestream velocity from the raw vector data. Vectors in this frame of reference result from the influence of the stationary moth's body and the unsteady influence of the beating wings. The first local frame of reference is only strictly valid around the stationary body (i.e. at the centreline), and is generated by subtracting the freestream after deflection by the head and thorax. Vectors in this frame of reference result from the unsteady influence of the moth's beating wings. The second local frame of reference is an unsteady one, and is only strictly valid around the wings away from the influence of the body. It is generated by subtracting both the freestream and the wing's own motion from the raw vector data. Vectors in this frame of reference result from the unsteady influence of the moth's beating wings, and are those seen by an observer moving with the wing.

The first frame of reference involves no adjustment of the raw data. The second and third frames of reference involve subtraction of a uniform vector field, which cannot introduce a focus into a vector field where none existed previously. Nevertheless, a relatively small error in calculating the magnitude or direction of the uniform vector field could be enough to invalidate that frame of reference. In such cases, a real focus, which would be revealed in the velocity data set with correct vector transformation, can become skewed to the extent that it virtually disappears because the frame of reference has been assigned incorrectly. The fourth frame of reference involves subtracting a non-uniform vector field with non-zero rotation. This makes errors in calculating the vector field more problematic, because there is the potential not just to skew an existing focus, but to introduce a spurious focus where none really exists. In fact, as we show later, the magnitude of wing rotation in *Manduca* is sufficiently small with respect to rotation of the vortex that the correction to the frame of reference at supination is negligible, and none of the frames of reference that we actually use risks introducing a spurious rotation to the flow field.

Fig. 5 shows the effect of manipulating the vector field to remove the 3.5 m s^{-1} freestream velocity, with varying degrees of deflection by the body (from 0° to 25°, where the maximum angle is set by the profile of the thorax). The effects of each manipulation are described in the figure legend. With no freestream subtraction, (Fig. 5F), there is a noticeable kink in the streamlines as the flow deflects over the thorax, with a patch of colour marking an intense vorticity peak, but no focus is apparent. Subtracting the freestream reveals a focus in the streamlines, but the position of the focus does not coincide with the vorticity peak. Subtracting the deflected freestream shifts the focus relative to the vorticity peak: with 20° deflection, the focus coincides with the vorticity peak, strongly suggesting that this frame of reference is a locally valid one. Steeper angles of deflection skew and shift the focus so that it is displaced from the vorticity peak and eventually cause it to disappear altogether.

As is clear from Fig. 5, the process of subtracting the freestream can have profound impact on the shape of the streamlines, but has no effect on the distribution of vorticity. This is because vorticity is derived from shearing and divergence, neither of which is affected by the manipulation. In practice we subtracted a constant vector value of the freestream from the images. In every vector field where a focus was present in the frame of reference defined by this manipulation, the focus always coincided with a vorticity peak, providing further confirmation that the frames of reference we are identifying are valid. In almost all cases, the frame of reference identified in this way turned out to be a frame of reference fixed relative to the freestream. This seems to be logically correct for centreline images, because the only movement now visible in the DPIV vector maps is due to the influence of the moth. We can only see the LEV at the bottom of the wingbeat (because the LEV is obscured behind the wing at other times). Then, the wing is stationary or only slowly rotating, so that subtracting the freestream also provides a valid frame of reference relative to the wings. This would not be true mid-downstroke, for example, when the wing velocity greatly exceeds the freestream velocity.

No rotation was added to the matrix in any of our analyses so streamlines that converge into a focus are a real phenomenon in the chosen frame of reference. It could be argued that the true frame of reference relative to the midwing position should be fixed relative to the wing. If we were to use a rotating frame of reference of this kind the effect would be to increase the circulation in the LEV without shifting its position or changing its size. Wing rotation varied from 0° to 1.5° in the 200 μs interval between frames in the analysed data, translation was negligible in every analysed image. In the worst case this corresponds to a rotation rate about the wing rotational axis of 5500 deg. s^{-1}, which would contribute a change in velocity at the edge of the LEV core of less than 0.1 m s^{-1}, an order of magnitude less than the velocity actually measured at the edge of the vortex core. By ignoring the supinatory wing rotation whilst assigning the frame of reference, we decrease the strength of the measured LEV because the direction of rotation of wing and LEV is the same.

Results

The flow field induced by the moth towards the end of the downstroke at the beginning of supination is shown in Fig. 6. We have assumed a frame of reference fixed with respect to the 3.5 m s^{-1} freestream. The flow halfway out along the wings (Fig. 6A,B) is separated at the leading edge and the instantaneous streamlines converge in a stable focus above the wing at about the quarter chord point. This focus coincides with a vorticity maximum, demonstrating both that this frame of reference is valid, and that there is a vortex above the wing in a position close behind the leading edge. The timing of this DPIV image coincides with the period of peak upward dynamic force production, and at the instant shown in the image the total upwards force is equivalent to 2.2 times body weight (Fig. 6C). Fig. 6C helps to put the LEV images into the context of the whole wingstroke. Inertial forces have not been removed from the force traces, because it was not possible to obtain sufficiently detailed wing kinematics for calculating the inertial forces at the same time as making DPIV measurements, and there are no published wingbeat kinematics for *Manduca sexta* of sufficient resolution to allow us to estimate inertial forces. However, since the wings decelerate in preparation for stroke reversal, inertial forces must be acting downwards, so the aerodynamic contribution must be greater than the measured value. The forces are presented here only to show the correspondence in time between the dynamic force produced by the insect and the LEV measured by DPIV. The total force production during a wingbeat and rate of momentum transport into the wake are dealt with in detail elsewhere (Bomphrey, 2004; R. J. Bomphrey, N. J. Lawson, G. K. Taylor and A. L. R. Thomas, manuscript in preparation).

The vortex structure seen above the wing in Fig. 6 is present in all DPIV images showing this area of the flow field, and the position and sign of the focus above the wing at about the quarter chord point is consistent with previous studies of the flow field around insect wings describing LEVs. However, Fig. 7 shows the flow over the centreline of the thorax in five images taken at 3.5 m s^{-1}. In each case there is a vorticity peak above and slightly aft of the thorax. This suggests the presence of a vortex above the centreline as well as above the midwing position. The same structure occurs consistently in flight at 1.2 m s^{-1} at the centreline and midwing positions. Our DPIV with tethered *Manduca* shows the LEV above the centreline, and at the midwing in all flight sequences at each of the two flight speeds. Three of the example DPIV images shown in Fig. 7 exhibit further patches of vorticity, particularly what appears to be a pair of opposite sign close to the upstream (left) side of the field of view. These patches are not as strong as the LEV, nor are they consistent between wingbeats. During the experimental sessions the position in which the subject held its antennae occasionally changed. It could be that these patches

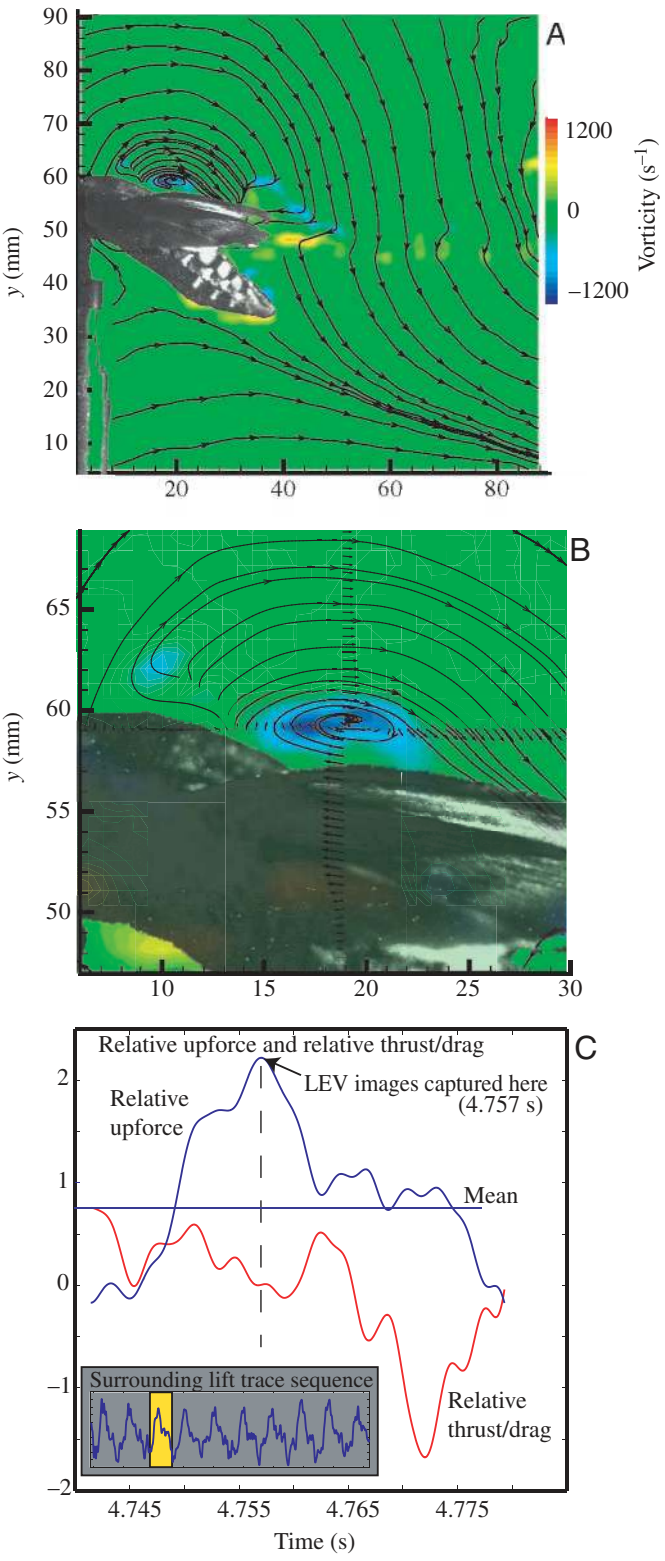

Fig. 6. The late downstroke leading-edge vortex (LEV) of *Manduca sexta*. Flow fields resolved after subtraction of the freestream velocity (3.5 m s^{-1}). (A,B) Vorticity and streamlines in the wake and near-wing flow field of *Manduca*, shown to provide context. (A) The vortex sheet is shed from the trailing edge of the wings; (B) how the streamlines spiral into a stable focus at a midwing location, just above the leading edge. (C) Two excerpts from the corresponding force trace, with the output normalised relative to body weight. The instant the three images were taken is shown by a broken line at the peak in relative upforce (2.2 times that required to support body weight).

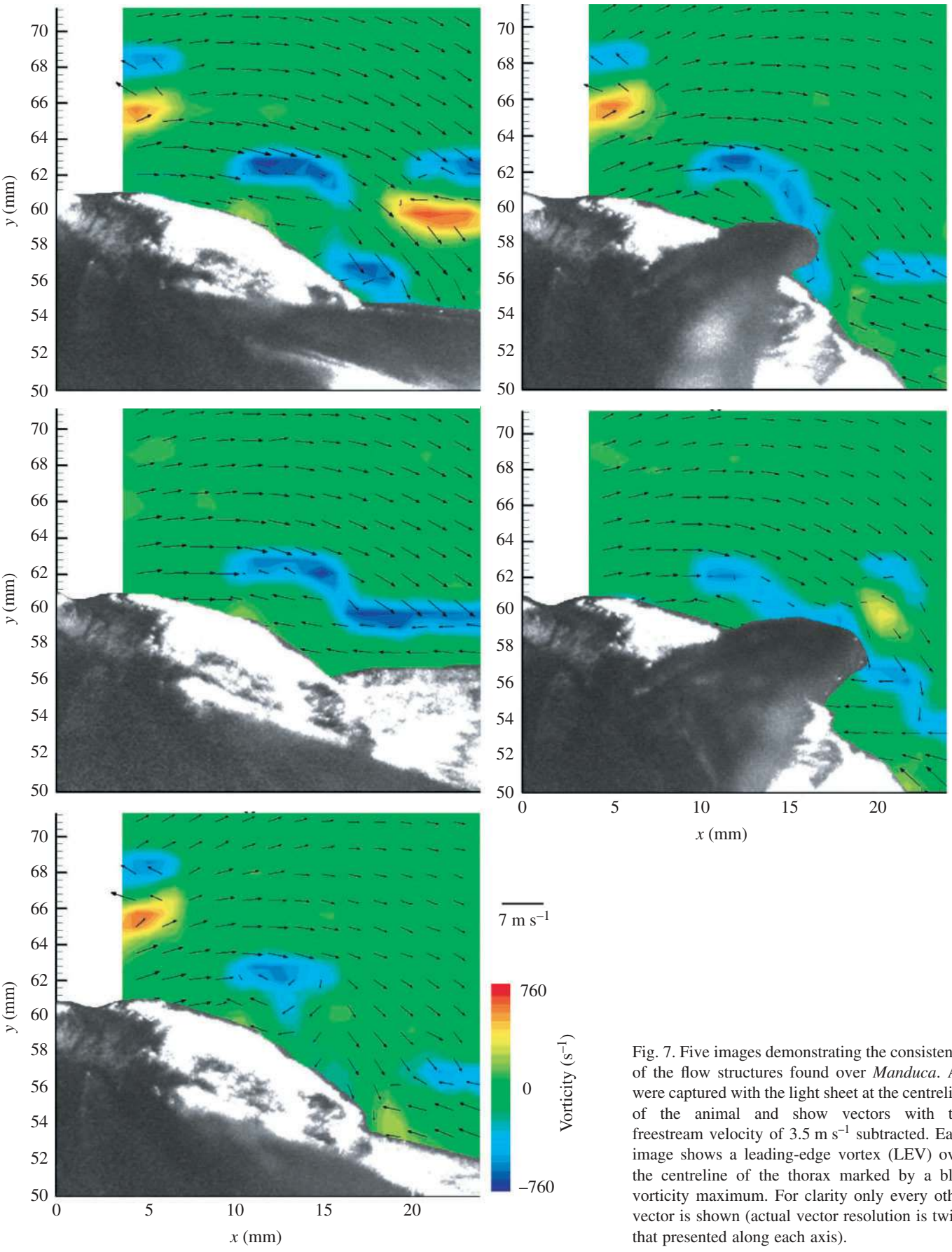

Fig. 7. Five images demonstrating the consistency of the flow structures found over *Manduca*. All were captured with the light sheet at the centreline of the animal and show vectors with the freestream velocity of 3.5 m s^{-1} subtracted. Each image shows a leading-edge vortex (LEV) over the centreline of the thorax marked by a blue vorticity maximum. For clarity only every other vector is shown (actual vector resolution is twice that presented along each axis).

of vorticity are a result of shearing in the wake shed from the antennae. However, no manipulation of the frame of reference could provide streamlines which spiralled in towards a stable focus for these extraneous patches of vorticity – therefore they do not satisfy the requirements we use here to define a vortex.

Fig. 8 shows the velocity profiles and vorticity profiles in vertical transects through the LEVs on three separate wingbeats at 1.2 m s^{-1} and at 3.5 m s^{-1}. Four features of the LEV revealed in Fig. 8 are especially notable. Firstly, the vortex structure identified in each of these twelve images is remarkably consistent, both in position and in size (the small vertical jitter in the vorticity profiles is due to slight differences in wing position between images). Secondly, the velocity and vorticity profiles are entirely consistent with the structure

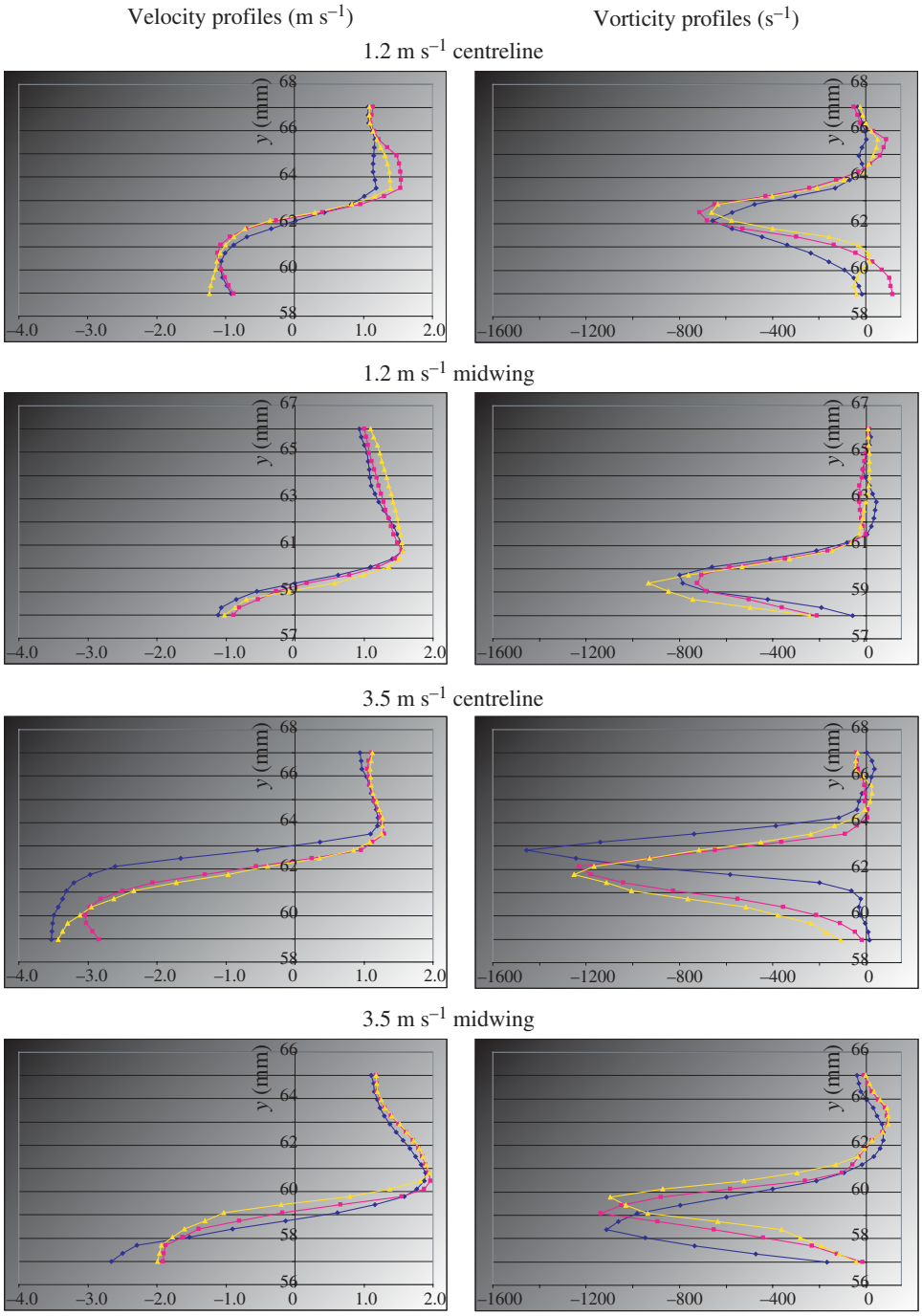

Fig. 8. Velocity profiles (left) and vorticity profiles (right) in vertical transects through the LEV after simple freestream subtraction. Three separate wingbeats at each of the two flight speeds (1.2 m s^{-1} and 3.5 m s^{-1}) with the light sheet at the centreline and midwing positions. In each case the peak in vorticity coincides with the centre of the portion of the velocity profiles, which are associated with solid body rotation of the vortex core. Each transect represents the horizontal component of the velocity vector, i.e. the component parallel with the freestream.

expected in a vortex core. Thirdly, the DPIV data are consistent right into the centre of the vortex core both at the centreline and at midwing in each of the images. Fourthly, the strength of the LEV is greater in terms of vorticity at the higher speed than at the lower speed, but the LEV core diameter does not differ at the two speeds.

The velocity profiles show that the peak velocity at the outer edge of the LEV is 2.6 times the freestream in the 1.2 m s^{-1} case and 1.4 times the freestream in the 3.5 m s^{-1} case (v_{max}/U, where v_{max} is the maximum velocity at the edge of the vortex core and U is the freestream velocity). This large velocity increase around the LEV demonstrates that the LEV is generated (or at least augmented) by an active process, which can only be a result of the influence of the flapping wings at the centreline. For comparison, passive roll-up and subsequent vortex shedding from circular cylinders at Reynolds numbers from 100 to 100×10^3 lead to a maximum velocity increase in the shed vortices of only 1.2 times the freestream velocity. Hypothetical cylinders with diameters based on the thorax, head, or both, of a hawkmoth flying at these speeds fall comfortably within this range of Reynolds number; other shapes, such as the roughly spherical head, or the roughly ellipsoidal body, would be expected to shed vortices with still lower maximum velocities. For a detailed parametric study, and a collation of similar works, see Zdravkovich (1997).

Previous work suggested that the LEV increased in size with speed (Ellington et al., 1996; Willmott et al., 1997). Our DPIV results do not support this conclusion. At 1.2 m s^{-1}, at the centreline the measured mean vortex core diameter (d) was 3.0±0.2 mm (mean ± S.D.) and mean tangential velocity (v) at the edge of the vortex core was 1.24±0.10 m s^{-1} (mean ± S.D.). The circulation, $\Gamma=\pi dv$, is 0.012±0.001 m^2 s^{-1} (mean ± S.D.) at the centreline and 0.011±0.001 m^2 s^{-1} at midwing. The lift per unit span (L) is given by $L=\rho U\Gamma$ (where ρ is air density, 1.225 kg m^{-3}; and U is incident freestream velocity, 1.2 m s^{-1}), so assuming the circulation measured at this instant is maintained across the whole span (0.112 m wingtip to wingtip), then the LEV alone could support 2.0 mN at this flight speed, which corresponds to 13.4% of body weight.

At 3.5 m s^{-1} (U=3.5 m s^{-1}) LEV circulation is 0.011±0.0004 m^2 s^{-1} at the centreline and 0.020±0.004 m^2 s^{-1} at the midwing position. These LEV circulations could contribute a lift force somewhere between 5.3 mN (based on the circulation at centreline) and 9.6 mN (based on the circulation at the midwing) – i.e. supporting between 35.6% and 64.7% of body weight. The circulation is higher at midwing than at the centreline at 3.5 m s^{-1} but the core diameter is not significantly larger (3.1±0.75 mm rather than 2.8±0.75 mm). At 1.2 m s^{-1} the diameter is the same, 3.0±0.75 mm at the centreline and 2.8±0.75 mm at the midwing. The circulation is marginally higher at the centreline than the midwing. The diameter of the LEV is approximately 10% of the local wing chord. Caution should be taken in the calculation of lift production from the LEV because it is based on the freestream velocity, whereas a more sophisticated calculation would also include the component of the wing's motion. As the data were collected close to stroke reversal, that component has been considered negligible relative to the more dominant flow velocity component provided by the freestream.

These data give a gross estimate of the amount of lift the LEV could be contributing, show unequivocally that the LEV is continuous across the centreline late in the downstroke, and suggest that the LEV doesn't change much in size or strength at the two measurement sites at the two speeds. However, they do not allow us to provide a detailed description of the minor variation in the size and shape of the LEV with speed, or across the span. 3D DPIV data with high temporal and spatial resolution would allow refinement of this description.

The flow features identified by DPIV above the wing of our tethered *Manduca* are consistent with a Class II LEV structure, topologically equivalent to that recently identified in dragonflies (Thomas et al., 2004), free-flying butterflies (Srygley and Thomas, 2002), and hawkmoths (Luttges, 1989). The simplest explanation of the measured topology assumes that the centreline and midwing flow fields are simply connected (they are only about 2 cm apart). If so, then there is a LEV that runs above approximately the quarter chord point of the wings, parallel to the leading edge of the wings and across the thorax. The LEV is continuous with the wingtip vortices, as shown in previous work with *Manduca* (Willmott et al., 1997). A cartoon of this flow structure is shown in Fig. 9.

The DPIV results for this stage of the wingbeat are not consistent with the Class III interpretation of the LEV structure in *Manduca* presented in previous studies. Nor are they consistent with the Class I LEV, because incident streamlines curving over the thorax reattach further aft on the surface of the thorax or abdomen (Fig. 9). The vortex is therefore still considered bound to the animal even at this late stage of the wingbeat. It is this feature that distinguishes the Class I and Class II LEVs. The Class I LEV flow field described by Maxworthy (1979) has yet to be visualised on a real insect, but wing-root vortices of the sort he described might perhaps be expected on insects with strongly petiolated wings such as are found in some Diptera and Hymenoptera, and were a feature of his model flapper.

Discussion

During the late downstroke of *Manduca*, the flow separates at, or near, the leading edge of the wing. Flow separation is associated with a particular kind of critical point called a saddle, which in this case must exist between the wing bases, on the surface of the thorax. The rules of critical point theory (Lighthill, 1963) require that there be two more nodes than saddles on a surface in a flow. There are therefore, in the simplest physically consistent topological structure, three nodes: a node of attachment (forward stagnation point) on the head, a node of detachment (rearward stagnation point) at the tip of the abdomen, and between these, a node of reattachment where the separation surface bounding the LEV reattaches to the thorax. The DPIV technique that we employed is ideally suited to identifying free-slip critical points such as the foci we

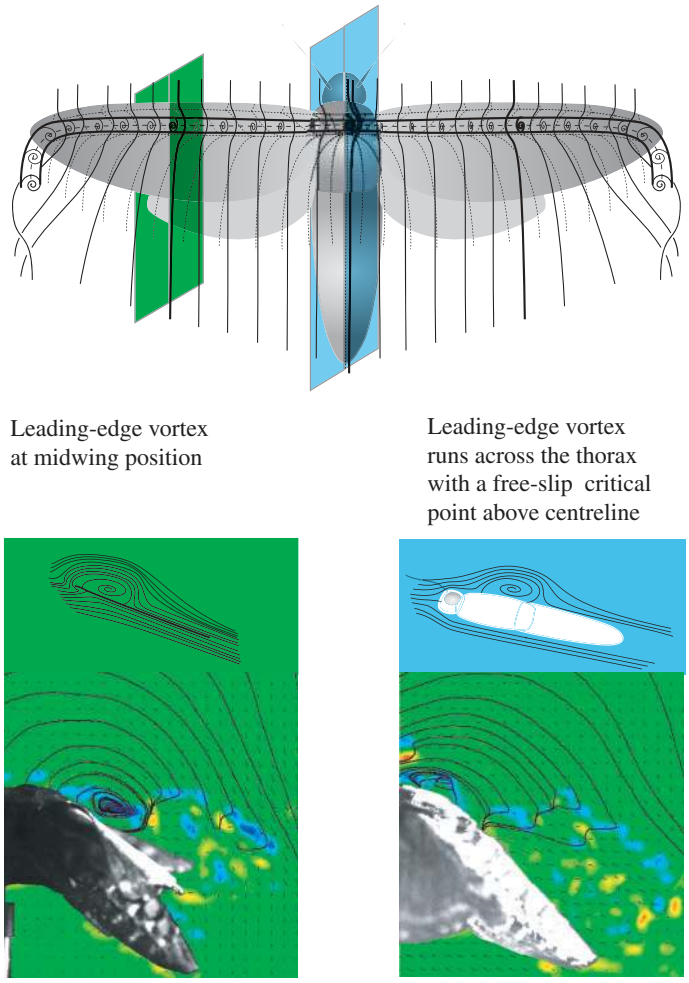

Fig. 9. Cartoon showing the aerodynamic features of a Class II LEV in the flow around the wings and thorax of *Manduca sexta* in late downstroke (top). DPIV inserts (bottom) show typical flow fields at each location with a freestream of 3.5 m s^{-1}. The midwing insert (left) has simple (horizontal) freestream subtraction; the centreline insert (right) has local freestream subtraction of 3.5 m s^{-1} angled 1° below horizontal.

have identified above *Manduca*. DPIV is not suited to identifying surface-bound critical points on a live flying insect, where glare is an issue, contrast is low, and many of the surfaces are obscured. The critical point description that we assume above is the simplest topological model that is both consistent with the presence of a free-slip focus, and that obeys the rules of critical point theory (Srygley and Thomas, 2002; Thomas et al., 2004).

Visualisations of the flow over the thorax are essential in order to determine the topology of the LEV. It is therefore unsurprising that some previous studies of *Manduca* have identified a different vortex structure from the one we find in this study, because they did not visualise centreline flows. Moreover, studies on large-scale mechanical flappers usually incorporate a sizable gap between the wing bases (Ellington et al., 1996; Maxworthy, 1979; Van den Berg and Ellington, 1997a), which will minimise wing interaction and diminish the likelihood of a continuous LEV. Conical (Class III) LEVs are to be expected on flappers of this kind, and may occur on real insects, but we did not find evidence for that structure using DPIV to look at the late downstroke of *Manduca*. On mechanical flappers or plungers with continuous wing surfaces, operating at appropriate Strouhal numbers, the LEV is continuous across the centreline (Thomas et al., 2004).

Early work suggested that spanwise flow was necessary for the stability of conical LEVs (Ellington et al., 1996; Maxworthy, 1979). Spanwise flows are inevitable wherever there is a focus at the core of the LEV because the focus is acting as a sink, and flow reaching the centre of the focus must be transported away somehow; the key question, however, is whether the spanwise flow is necessary for LEV stability, and has sufficient velocity to transport away vorticity that would otherwise cause the LEV to grow and become unstable (Ellington et al., 1996). Recent studies have shown stable LEVs over a flapping wing scaled to the lower Reynolds numbers associated with *Drosophila* flight, even when fences stopped any spanwise flow (Birch and Dickinson, 2001). In dragonflies spanwise flows are so weak that they often could not be detected by smoke visualisation but, when present, spanwise flows could be driven by sideslip to run in either direction along the wings (Thomas et al., 2004).

Two-dimensional DPIV can only directly measure u and v (in-plane) velocity components along the x and y axes (defined by the camera's frame of reference). So with our cameras aligned so that x and y are perpendicular to the LEV axis, our 2D DPIV cannot directly measure the flow velocity along that axis. However, the laser light sheet thickness and pulse separation allow us to place upper limits on the velocity of any spanwise flows. If the laser pulse separation was too high, spanwise flows would take particles out of the lightsheet causing data dropout. The pulse separation was chosen to limit the maximum particle displacement between pulses to less than 30% of the light sheet thickness, which minimises data dropout while maximising measurement accuracy (Keane and Adrian, 1991). As no major areas of data dropout were observed in the LEV region, spanwise flow cannot have exceeded the limit set in the experiments. The light sheet thickness was 0.5 mm, so it can be concluded that with a pulse separation of 120 µs at the freestream velocity of 3.5 m s^{-1} the upper limit on spanwise velocity in the LEV is 1 m s^{-1}, and with 200 µs pulse separation at the freestream velocity of 1.2 m s^{-1} the upper limit on spanwise flow velocity is 0.4 m s^{-1}.

Other studies (Maxworthy, 1979; van den Berg and Ellington, 1997) have inferred that LEVs used by insects are analogous in some respects to those found on delta wing aircraft. In particular, it has been suggested that the LEV may be stabilised by a strong axial flow toward the wing tip. Van den Berg and Ellington estimated that the axial flow on their robotic hawkmoth was of the same magnitude as the swirl (speed of rotation around the vortex axis). Given the presence

of a centreline LEV observed here, and the associated flow topology, the spanwise velocity component during *Manduca*'s late downstroke is likely to be significantly less than the spanwise flow in the LEV on a delta wing. For example, on a 60° apical angle delta wing at 30° angle of attack, the flow velocity along the LEV core would be (by trigonometry) about 75% of the freestream velocity – at least 2.5 times greater than the maximum spanwise flow that would still allow us to resolve data with our 2D DPIV system. 3D stereoscopic DPIV data (Prasad, 2000) is required to measure such spanwise velocities along the vortex core to conclusively quantify this flow characteristic.

It may be the case that spanwise flow is not necessary for vortex stabilisation on a plunging aerofoil. A delta wing can be considered to be continuously plunging (pp. 140–145 in Jones, 1990), constantly building up vorticity as it does so, until that vorticity becomes too much for the LEV to remain stably over the wing without some sort of vorticity sink to prevent shedding. Theoretical (Lewin and Haj-Hariri, 2003; Triantafyllou et al., 1991; Wang, 2000) and experimental (Triantafyllou et al., 1993; Taylor et al., 2003) analyses suggest that swimming and flying animals, including *Manduca,* operate in a Strouhal number range where an LEV is expected to remain bound to the wing for the entire duration of the wingbeat. Provided the timescale of the wingbeat is shorter than the timescale on which the accumulating vorticity causes the vortex to be shed, the LEV can be stable for the duration of the downstroke, even with negligible spanwise flow (Wang et al., 2004). Moreover, operating in the appropriate Strouhal number range ($0.2<St<0.4$) has been shown in inviscid (Wang, 2000) and viscous flow models (Lewin and Haj-Hariri, 2003) to provide maximum propulsive power efficiency (output propulsive power in the wake over input propulsive power from the muscles), so spanwise flow may not be important for animals whose wing kinematics are configured to optimise propulsive efficiency.

Flow visualisations with free-flying butterflies (Srygley and Thomas, 2002), and free-flying and tethered dragonflies (Bomphrey et al., 2002; Thomas et al., 2004) all reveal the same LEV structure: an LEV that extends from wingtip vortex to wingtip vortex and is continuous across the centreline. Our DPIV results with tethered *Manduca* show a similar structure late in the stroke, once the LEV lifts off across the thorax, but prior to that the wings obscure the flow field. At this stage, we can only speculate on the quantitative flow topology over the thorax early in the wing stroke. Our smoke visualisations suggest that for at least the first half of the downstroke the structure matches that described by Ellington et al. (1996) and Willmott et al. (1997) but, until the flow field is analysed quantitatively, the flow topology will remain only partially described. It is conceivable that early in the downstroke the flow separates over the wings while remaining attached over the thorax, resembling a conical Class III LEV, then later separates over the thorax and becomes the Class II LEV observed here. After stroke reversal, with the wings into the upstroke, the vortex may shed from the thorax first, restoring attached flow in this region; if this were the case it would give rise to a transitional stage resembling the Class I LEV. Higher temporal resolution (combined with a varying camera position to give continuous views throughout the wingbeat) would elucidate the finer detail of LEV formation and shedding in *Manduca*, in particular lending support to which, if any, are the dominant flow patterns, and which, if any, are merely transitional states.

R.J.B. was supported during this work by a BBSRC DPhil Studentship. G.K.T. is supported by a Royal Society University Research Fellowship, and was supported during this work by a Royal Commission for the Exhibition of 1851 Research Fellowship, a Weir Junior Research Fellowship at University College, Oxford, and a Christopher Welch Scholarship. A.L.R.T. was supported by a Royal Society University Research Fellowship.

References

Banks, D. C. and Singer, B. A. (1995). A predictor-corrector technique for visualizing unsteady-flow. *Ieee Trans. Vis. Comp. Graphics* **1**, 151-163.

Birch, J. M. and Dickinson, M. H. (2001). Spanwise flow and the attachment of the leading-edge vortex on insect wings. *Nature* **412**, 729-733.

Bomphrey, R. J. (2004). The aerodynamics of insect flight. DPhil thesis, University of Oxford.

Bomphrey, R. J., Srygley, R. B., Taylor, G. K., Nudds, R. L. and Thomas, A. L. R. (2002). Visualising the flow around insect wings. *Phys. Fluids* **14**, S4.

Délery, J. M. (2001). Robert Legendre and Henri Werlé: Toward the elucidation of three-dimensional separation. *Ann. Rev. Fluid Mech.* **33**, 129-154.

Dickinson, M. H., Lehmann, F.-O. and Sane, S. P. (1999). Wing rotation and the aerodynamic basis of insect flight. *Science* **284**, 1954-1960.

Ellington, C. P., van den Berg, C., Willmott, A. P. and Thomas, A. L. R. (1996). Leading-edge vortices in insect flight. *Nature* **384**, 626-630.

Gad-el-Hak, M. and Ho, C.-M. (1985). The pitching delta wing. *AIAA J.* **23**, 1660-1665.

Gursul, I., Lin, H. and Ho, C.-M. (1994). Effects of time scales on lift of airfoils in an unsteady stream. *AIAA J.* **32**, 797-801.

Hama, F. R. (1962). Streaklines in a perturbed shear flow. *Phys. Fluids* **5**, 644-650.

Hart, D. P. (2000). PIV error correction. *Exp. Fluids* **29**, 13-22.

Huang, M.-K. and Chow, C.-Y. (1982). Trapping of a free vortex by Joukowski airfoils. *AIAA J.* **20**, 292-298.

Jones, K. D. and Platzer, M. E. (1996). Time-domain analysis of low-speed airfoil flutter. *AIAA J.* **34**, 1027-1033.

Jones, R. T. (1990). *Wing Theory.* New Jersey: Princeton University Press.

Keane, R. D. and Adrian, R. J. (1991). Optimization of particle image velocimeters. II. Multiple pulsed systems. *Measurement Sci. Tech.* **2**, 963-974.

Kliss, M., Somps, C. and Luttges, M. W. (1989). Stable vortex structures: a flat plate model of dragonfly hovering. *J. Theor. Biol.* **136**, 209-228.

Lawson, N. J. and Davidson, M. R. (2001). Self-sustained oscillation of a submerged jet in a thin rectangular cavity. *J. Fluids Struct.* **15**, 59-81.

Lewin, G. C. and Haj-Hariri, H. (2003). Modelling thrust generation of a two-dimensional heaving airfoil in a viscous flow. *J. Fluid Mech.* **492**, 339-362.

Lighthill, M. J. (1963). Attachment and separation in three-dimensional flow. In *Laminar Boundary Layers* (ed. L. Rosenhead), pp. 72-82. Oxford: Clarendon Press.

Lugt, H. J. (1985a). Vortex flow and maximum-principles. *Am. J. Phys.* **53**, 649-653.

Lugt, H. J. (1985b). Vortices and vorticity in fluid dynamics. *Am. Sci.* **73**, 162-167.

Luttges, M. (1989). Accomplished insect fliers. In *Frontiers In Experimental Fluid Mechanics* (ed. M. Gad-el-Hak), pp. 429-456. Berlin: Springer.

Maxworthy, T. (1979). Experiments on the Weis-Fogh mechanism of lift

generation by insects in hovering flight. Part 1. Dynamics of the 'fling'. *J. Fluid Mech.* **93**, 47-63.

Maxworthy, T. (1981). The fluid-dynamics of insect flight. *Annu. Rev. Fluid Mech.* **13**, 329-350.

Mourtos, N. J. and Brooks, M. (1996). Flow past a flat plate with a vortex/sink combination. *J. Appl. Mech.* **63**, 543-550.

Perry, A. E. and Chong, M. S. (2000). Interpretation of flow visualization. In *Flow Visualisation: Techniques and Examples* (ed. A. J. Smits and T. T. Lim), pp. 1-26. London: Imperial College Press.

Prasad, A. J. (2000). Stereoscopic particle image velocimetry. *Exp. Fluids* **29**, 103-116.

Reavis, M. A. and Luttges, M. W. (1988). Aerodynamic forces produced by a dragonfly. *AIAA Paper* 88-0330.

Reeves, M. and Lawson, N. J. (2003). Evaluation and correction of perspective errors in endoscopic PIV. *Exp. Fluids* **36**, 701-705.

Riddle, T. W., Wadcock, A. J., Tso, J. and Cummings, R. M. (1999). An experimental analysis of vortex trapping techniques. *J. Fluids Eng.* **121**, 555-559.

Robinson, S. K. (1991). Coherent motions in the turbulent boundary-layer. *Annu. Rev. Fluid Mech.* **23**, 601-639.

Rossow, V. J. (1978). Lift enhancement by an externally trapped vortex. *J. Aircraft* **15**, 618-624.

Rossow, V. J. (1992). Two-fence concept for efficient trapping of vortices on airfoils. *J. Aircraft* **29**, 847-855.

Rossow, V. J. (1994). Aerodynamics of airfoils with vortex trapped by two spanwise fences. *J. Aircraft* **31**, 146-153.

Saffman, P. G. and Sheffield, J. S. (1977). Flow over a wing with an attached free vortex. *Stud. Appl. Math.* **57**, 107-117.

Sane, S. P. and Dickinson, M. H. (2002). The aerodynamic effects of wing rotation and a revised quasi-steady model of flapping flight. *J. Exp. Biol.* **205**, 1087-1096.

Somps, C. and Luttges, M. (1985). Dragonfly flight – novel uses of unsteady separated flows. *Science* **228**, 1326-1329.

Srygley, R. B. and Thomas, A. L. R. (2002). Unconventional lift-generating mechanisms in free-flying butterflies. *Nature* **420**, 660-664.

Taylor, G. K., Nudds, R. L. and Thomas, A. L. R. (2003). Flying and swimming animals cruise at a Strouhal number tuned for high power efficiency. *Nature* **425**, 707-711.

Thomas, A. L. R., Bomphrey, R. J., Srygley, R. B., Nudds, R. L. and Taylor, G. K. (2004). Dragonfly flight: free-flight and tethered flow visualizations reveal a diverse array of unsteady lift generating mechanisms, controlled primarily via angle of attack. *J. Exp. Biol.* **207**, 4299-4323.

Triantafyllou, G. S., Triantafyllou, M. S. and Grosenbaugh, M. A. (1993). Optimal thrust development in oscillating foils with application to fish propulsion. *J. Fluids Struct.* **7**, 205-224.

Triantafyllou, M. S., Triantafyllou, G. S. and Gopalkrishnan, R. (1991). Wake mechanics for thrust generation in oscillating foils. *Phys. Fluids A* **3**, 2835-2837.

Tuncer, I. H. and Platzer, M. F. (1996). Thrust generation due to airfoil flapping. *AIAA J.* **34**, 324-331.

Usherwood, J. R. and Ellington, C. P. (2002). The aerodynamics of revolving wings – I. Model hawkmoth wings. *J. Exp. Biol.* **205**, 1547-1564.

Van den Berg, C. and Ellington, C. P. (1997a). The three-dimensional leading-edge vortex of a 'hovering' model hawkmoth. *Phil. Trans. R. Soc. Lond. B* **352**, 329-340.

Van den Berg, C. and Ellington, C. P. (1997b). The vortex wake of a 'hovering' model hawkmoth. *Phil. Trans. R. Soc. Lond. B* **352**, 317-328.

Wang, Z. J. (2000). Vortex shedding and frequency selection in flapping flight. *J. Fluid Mech.* **410**, 323-341.

Weis-Fogh, T. (1973). Quick estimates of flight fitness in hovering animals, including novel mechanisms for lift production. *J. Exp. Biol.* **59**, 169-230.

Willmott, A. P., Ellington, C. P. and Thomas, A. L. R. (1997). Flow visualization and unsteady aerodynamics in the flight of the hawkmoth, *Manduca sexta*. *Phil. Trans. R. Soc. Lond. B* **352**, 303-316.

Zbikowski, R. (2002). On aerodynamic modelling of an insect-like flapping wing in hover for micro-air vehicles. *Phil. Trans. R. Soc. Lond. A* **360**, 273-290.

Zdravkovich, M. M. (1997). *Flow Around Circular Cylinders*. New York: Oxford University Press.